ARTICLES
PUBLISHED ONLINE: 7 AUGUST 2011 | DOI: 10.1038/NMAT3087
nature materials

Co_3O_4 nanocrystals on graphene as a synergistic catalyst for oxygen reduction reaction

Yongye Liang[1†], Yanguang Li[1†], Hailiang Wang[1†], Jigang Zhou[2], Jian Wang[2], Tom Regier[2] and Hongjie Dai[1*]

Catalysts for oxygen reduction and evolution reactions are at the heart of key renewable-energy technologies including fuel cells and water splitting. Despite tremendous efforts, developing oxygen electrode catalysts with high activity at low cost remains a great challenge. Here, we report a hybrid material consisting of Co_3O_4 nanocrystals grown on reduced graphene oxide as a high-performance bi-functional catalyst for the oxygen reduction reaction (ORR) and oxygen evolution reaction (OER). Although Co_3O_4 or graphene oxide alone has little catalytic activity, their hybrid exhibits an unexpected, surprisingly high ORR activity that is further enhanced by nitrogen doping of graphene. The Co_3O_4/N-doped graphene hybrid exhibits similar catalytic activity but superior stability to Pt in alkaline solutions. The same hybrid is also highly active for OER, making it a high-performance non-precious metal-based bi-catalyst for both ORR and OER. The unusual catalytic activity arises from synergetic chemical coupling effects between Co_3O_4 and graphene.

Increasing energy demands have stimulated intense research on alternative energy conversion and storage systems with high efficiency, low cost and environmental benignity[1,2]. Catalysts for oxygen reduction and evolution reactions are at the heart of key renewable-energy technologies including fuel cells[3,4] and water splitting. Despite tremendous efforts, developing oxygen electrode catalysts with high activity at low cost remains a great challenge. The current bottleneck of fuel cells lies in the sluggish ORR on the cathode side[4]. Pt or its alloys are the best known ORR catalysts. Owing to the high cost of Pt and declining activity, alternative catalysts based on non-precious metals[5–7] and metal-free materials[8–10] have been actively pursued. On the other hand, the reverse reaction of ORR, OER or water oxidation plays an important role in energy storage such as solar fuel synthesis[2,11,12]. Ruthenium and iridium oxides in acidic conditions and first row spinel and perovskite metal oxides in basic conditions have been used to catalyse OER with moderate over-potentials (about 300–400 mV; ref. 13).

It is highly challenging but desirable to develop efficient bi-functional catalysts for both ORR and OER, particularly for unitized regenerative fuel cells, a promising energy storage system that works as a fuel cell and in reverse as a water electrolyzer producing H_2 and O_2 to feed the fuel cell[14,15].

Here, we show that Co_3O_4 nanoparticles, a material with little ORR activity by itself, when grown on reduced mildly oxidized graphene oxide (rmGO) exhibits surprisingly high performance in both ORR and OER in alkaline solutions. The hybrid exhibits comparable ORR catalytic activity to a commercial carbon-supported Pt catalyst (20 wt% Pt on Vulcan XC-72, Pt/C) and superior stability, thus leading to a new bi-functional catalyst for ORR and OER.

Co_3O_4/graphene hybrid was synthesized in solution[16–20] by a general two-step method. In the first step, Co_3O_4 nanoparticles were grown on mildly oxidized GO sheets (mGO) freely suspended in solution by hydrolysis and oxidation of cobalt acetate ($Co(OAc)_2$) at 80 °C (see Supplementary Information for details of the synthesis). Controlled nucleation of Co_3O_4 on mGO sheets was achieved by reducing the hydrolysis rate of $Co(OAc)_2$ by adjusting the ethanol/H_2O ratio and reaction temperature. Subsequent hydrothermal reaction at 150 °C led to crystallization of Co_3O_4 and reduction of mGO (signalled by a shift in the optical absorbance peak of graphene oxide (GO); refs 21,22) to form the Co_3O_4/rmGO hybrid. We also added NH_4OH in our synthesis steps to mediate hydrolysis of Co^{2+} and its oxidation[23], and obtained an N-doped hybrid material denoted as Co_3O_4/N-rmGO (see Supplementary Information). The amount of Co_3O_4 in our hybrid materials was ~70 wt% (~20 at% of Co), as revealed by thermal-gravimetric measurements.

Growth of Co_3O_4 nanocrystals on rmGO sheets was confirmed by scanning electron microscopy (SEM) for both Co_3O_4/N-rmGO (Fig. 1a) and Co_3O_4/rmGO (Supplementary Fig. S1a). Transmission electron microscopy (TEM) revealed smaller particles in Co_3O_4/N-rmGO (~4–8 nm in size, Fig. 1b) than Co_3O_4/rmGO (~12–25 nm in size, Supplementary Fig. S1b), attributed to NH_3 coordination with cobalt cations in reducing Co_3O_4 particle size[23,24] and enhanced particle nucleation on N-doped rmGO (N-rmGO). High resolution TEM showed the crystalline spinel structure of Co_3O_4 nanocrystals (Fig. 1c and Supplementary Fig. S1c), consistent with X-ray diffraction (XRD) data (Fig. 1d and Supplementary Fig. S1d). X-ray photoelectron spectroscopy (XPS) revealed 4 at% nitrogen in Co_3O_4/N-rmGO (Fig. 1e), but not in the Co_3O_4/rmGO sample made without NH_4OH (Supplementary Fig. S2a). In a control experiment, we verified that N-dopants were on reduced GO sheets (not in Co_3O_4 nanocrystals, see Supplementary Fig. S2b) by hydrothermal reactions between functional groups on mGO and NH_4OH in the solution[25]. High resolution XPS spectra of the N peak revealed pyridinic and pyrrolic nitrogen species in Co_3O_4/N-rmGO (Fig. 1e inset) and in N-rmGO (Supplementary Fig. S2c).

To assess their ORR catalytic activity, our materials were first loaded (with the same mass loading) onto glassy carbon electrodes

[1]Department of Chemistry, Stanford University, Stanford, California 94305, USA, [2]Canadian Light Source Inc., Saskatoon, Saskatchewan S7N 0X4, Canada.
[†]These authors contributed equally to this work. *e-mail: hdai@stanford.edu.

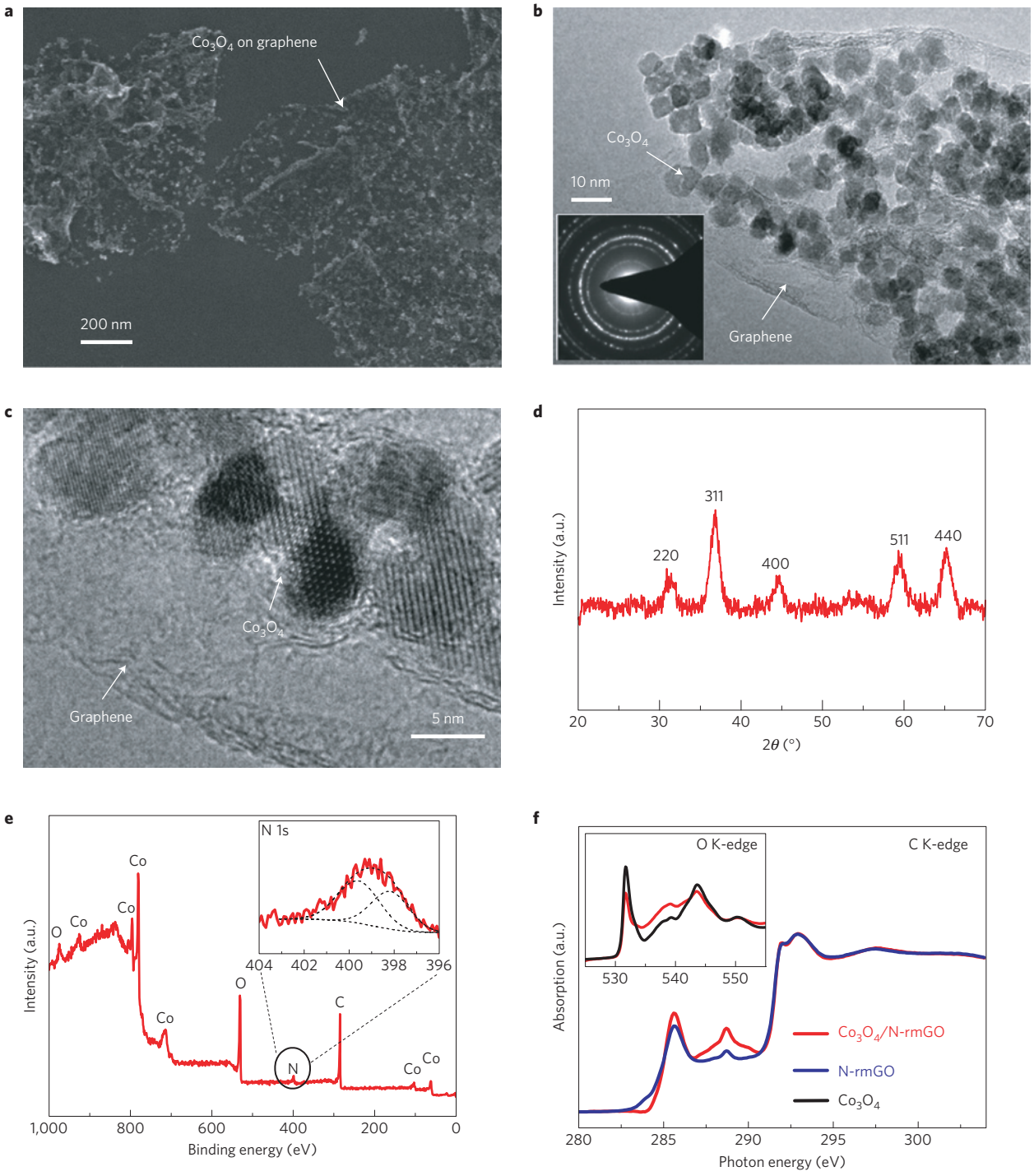

Figure 1 | Co_3O_4/graphene hybrid materials. a, Scanning electron microscopy image of Co_3O_4/N-rmGO hybrid deposited on a silicon substrate from a suspension in solution. **b**, Low magnification and **c**, high magnification TEM images of Co_3O_4/N-rmGO hybrid. **d**, XRD spectrum of a compacted film of Co_3O_4/N-rmGO hybrid. **e**, XPS spectrum of Co_3O_4/N-rmGO hybrid. Inset shows a high resolution N1s spectrum with the peak deconvoluted into pyridinic and pyrollic N peaks. **f**, C K-edge XANES of N-rmGO (blue curve) and Co_3O_4/N-rmGO hybrid (red curve). Inset shows O K-edge XANES of Co_3O_4 (black curve) and Co_3O_4/N-rmGO hybrid (red curve).

for cyclic voltammetry (CV) in O_2 versus Ar-saturated 0.1 M KOH (see Supplementary Information for experimental details). Free Co_3O_4 nanocrystals (size ~4–8 nm, similar to those grown on GO) or rmGO alone exhibited very poor ORR activity (Supplementary Fig. S3). Remarkably, the Co_3O_4/rmGO hybrid showed a much more positive ORR onset potential (~0.88 V relative to the reversible hydrogen electrode (RHE), see Supplementary Information for RHE calibration) and higher cathodic currents (Fig. 2a against Supplementary Fig. S3), suggesting synergistic ORR catalytic activity of Co_3O_4 and rmGO in the hybrid.

We used rotating-disk electrode (RDE) measurements to reveal the ORR kinetics of our Co_3O_4/rmGO hybrid in 0.1 M KOH (Fig. 2b). The linearity of the Koutecky–Levich plots and near parallelism of the fitting lines suggests first-order reaction kinetics toward the concentration of dissolved oxygen and similar electron transfer numbers for ORR at different potentials[26] (Fig. 2b

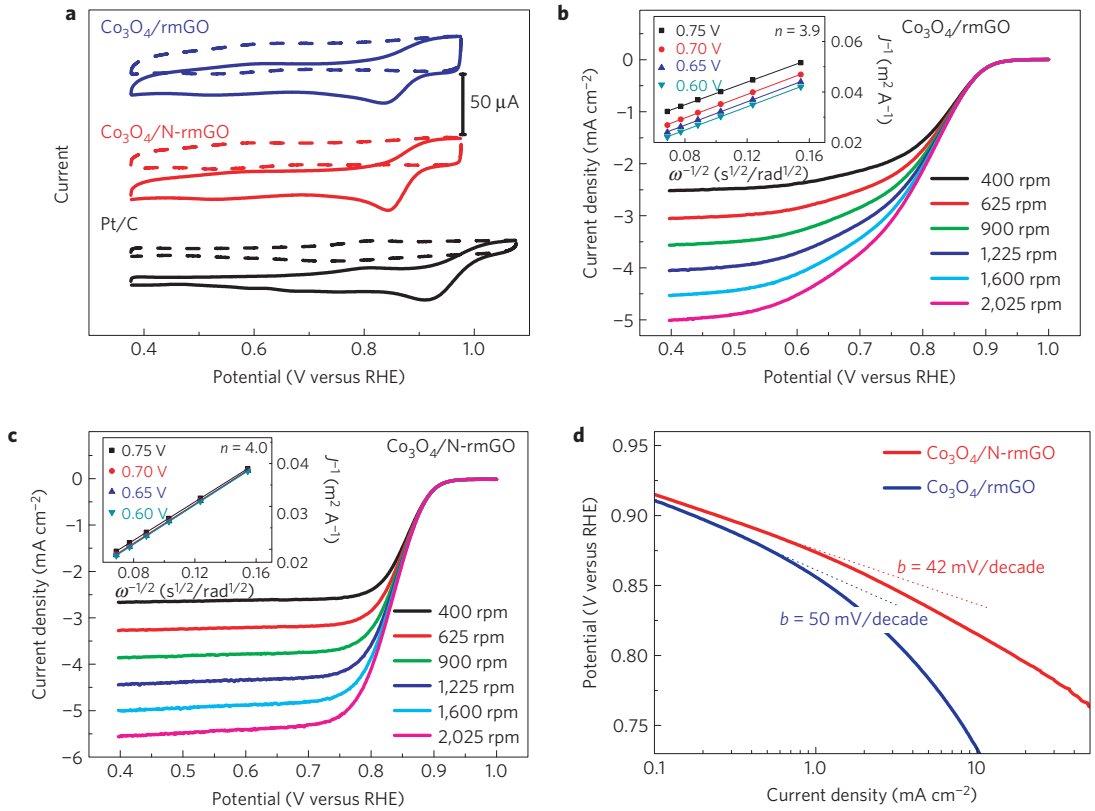

Figure 2 | Co_3O_4/graphene hybrid as oxygen reduction catalysts. a, CV curves of Co_3O_4/rmGO hybrid, Co_3O_4/N-rmGO hybrid and Pt/C on glassy carbon electrodes in O_2-saturated (solid line) or Ar-saturated 0.1 M KOH (dash line). Catalyst loading was 0.17 mg cm^{-2} for all samples. **b**, Rotating-disk voltammograms of Co_3O_4/rmGO hybrid (loading ~0.1 mg cm^{-2}) and **c**, Co_3O_4/N-rmGO hybrid (loading ~0.1 mg cm^{-2}) in O_2-saturated 0.1 M KOH with a sweep rate of 5 mV s^{-1} at the different rotation rates indicated. The insets in **b** and **c** show corresponding Koutecky–Levich plots (J^{-1} versus $\omega^{-0.5}$) at different potentials. **d**, Tafel plots of Co_3O_4/rmGO and Co_3O_4/N-rmGO hybrids derived by the mass-transport correction of corresponding RDE data (see Supplementary Information).

inset). The electron transfer number (n) was calculated to be ~3.9 at 0.60–0.75 V from the slopes of Koutecky–Levich plots[27] (Fig. 2b inset and see Supplementary Information), suggesting Co_3O_4/rmGO hybrid favours a 4*e* oxygen reduction process, similar to ORR catalysed by a high-quality commercial Pt/C catalyst measured in the same 0.1 M KOH electrolyte ($n \sim 4.0$ for Pt/C, see Supplementary Fig. S4a,b).

The performance of our hybrid catalyst was greatly enhanced with Co_3O_4/N-rmGO, made by adding NH_4OH during synthesis to afford N-doping in rmGO. The CV curve of Co_3O_4/N-rmGO hybrid exhibited a more positive ORR peak potential and higher peak current (Fig. 2a) than Co_3O_4/rmGO. RDE measurement revealed an electron transfer number of ~4.0 at 0.60–0.75 V (Fig. 2c). The half-wave potential at 1,600 r.p.m. was 0.83 V (Fig. 2c), similar to that of Pt/C (0.86 V; Supplementary Fig. S4a) and more positive than that of Co_3O_4/rmGO (0.79 V; Fig. 2b). Importantly, N-doped graphene (N-rmGO) alone, without Co_3O_4, exhibited low ORR activity (Supplementary Fig. S3) with an electron transfer number of ~2.7 at 0.50–0.65 V, suggesting a dominant 2*e* reduction process (Supplementary Fig. S5). Excellent ORR activity of the Co_3O_4/N-rmGO hybrid catalyst was also gleaned from the much smaller Tafel slope of 42 mV/decade at low over-potentials (Fig. 2d) than that measured with Co_3O_4/rmGO hybrid (54 mV/decade) in 0.1 M KOH.

To verify the ORR catalytic pathways of the hybrid materials, we performed rotating ring-disk electrode (RRDE) measurements to monitor the formation of peroxide species (HO_2^-) during the ORR process[28] (Fig. 3a). The measured HO_2^- yields are below ~12% and ~6% for Co_3O_4/rmGO and Co_3O_4/N-rmGO, respectively, over the potential range of 0.45–0.80 V, giving an electron transfer number of ~3.9 (Fig. 3b). This is consistent with the result obtained from the Koutecky–Levich plots based on RDE measurements, suggesting the ORR catalysed by our hybrids is mainly by 4*e* reduction.

We loaded our catalyst materials onto Teflon-treated carbon fibre paper (CFP) (at ~0.24 mg cm^{-2} for all samples) to measure their steady-state iR-compensated (i, cell current; R, nuisance resistor) polarization curves (Fig. 4). The Teflon-treated porous CFP is highly hydrophobic, providing a three-phase contact point for oxygen, electrolyte and catalyst[29] (known as the gas diffusion layer) useful in actual fuel cells to minimize the gas diffusion limitation[30,31]. In 0.1 M KOH at 0.7 V versus RHE (a typical half-cell cathodic potential in an operating fuel cell), our Co_3O_4/rmGO and Co_3O_4/N-rmGO hybrids afforded an ORR current density of ~12.3 mA cm^{-2} and ~52.6 mA cm^{-2} respectively (Fig. 4a), approaching that of the Pt/C catalyst (~68.0 mA cm^{-2}). The oxygen reduction currents of our hybrid catalysts were 1–3 orders of magnitude higher than Co_3O_4 (0.012 mA cm^{-2}), rmGO (0.19 mA cm^{-2}) or N-rmGO alone (3.5 mA cm^{-2}; Supplementary Fig. S6), further suggesting synergetic coupling effects between two catalytically non-active components in our hybrid for ORR catalysis.

In 1 M and 6 M KOH electrolytes, our Co_3O_4/N-rmGO ORR catalyst matched the performance of freshly loaded Pt/C catalyst in current density (Fig. 4b,c), accompanied by a positive shift in the ORR onset potential from 0.1 M KOH. The Tafel slope of kinetic current was down to ~37 mV/decade for Co_3O_4/N-rmGO in 1 M KOH (Supplementary Fig. S7), among the smallest Tafel slopes afforded by ORR catalysts. Importantly, our hybrid exhibits superior durability to Pt/C catalyst in 0.1–6 M KOH, with little

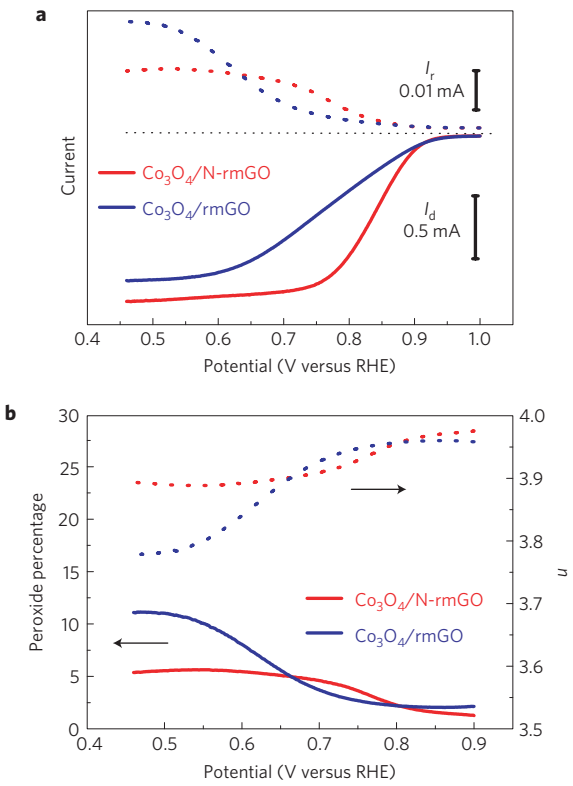

Figure 3 | Assessment of peroxide percentage in ORR catalysed by hybrid catalysts. a, Rotating ring-disk electrode voltammograms recorded with Co_3O_4/rmGO hybrid (loading ~0.1 mg cm^{-2}) and Co_3O_4/N-rmGO hybrid (loading ~0.1 mg cm^{-2}) in O_2-saturated 0.1 M KOH at 1,600 r.p.m. Disk current (I_d) (solid line) is shown on the lower half and ring current (I_r) (dotted line) is shown on the upper half of the graph. The disk potential was scanned at 5 mV s^{-1} and the ring potential was constant at 1.5 V versus RHE. **b**, Percentage of peroxide (solid line) and the electron transfer number (n) (dotted line) of Co_3O_4/rmGO and Co_3O_4/N-rmGO hybrids at various potentials, based on the corresponding RRDE data in **a**.

decay in ORR activity over 10,000–25,000 s of continuous operation (Fig. 4d–f). In contrast, the Pt/C catalyst exhibited 20%–48% decrease in activity in 0.1–6 M KOH (Fig. 4d–f), giving lower long-term ORR currents than the stable currents sustained by the Co_3O_4/N-rmGO hybrid catalyst.

We further compared the Co_3O_4/N-rmGO hybrid catalyst with other catalysts (Supplementary Fig. S8). Although the Pt/C – 50% (50 wt% Pt on Vulcan XC-72), a state-of-the-art Pt catalyst, showed slightly higher activity (Supplementary Fig. S8a), it suffered a significant 30% decrease in current density over 10,000 s of continuous operation in 1 M KOH (Supplementary Fig. S8b). A commercial Pd/C catalyst (10% Pd on activated carbon) showed lower activity than Co_3O_4/N-rmGO hybrid and obvious decay in activity over time (by ~20% in 10,000 s). Non-precious metal-N/C catalysts have shown excellent ORR activity in acidic[6] and in base[32,33] conditions. For comparison, we prepared a high quality Fe-N/C catalyst following refs 6,30 (see Supplementary Fig. S9 for RDE data). Notwithstanding a more positive onset potential, the Fe-N/C catalyst showed slightly lower activity than our Co_3O_4/N-rmGO hybrid at around 0.7 V. Furthermore, the Fe-N/C catalyst exhibited ~10% decreases in current density over 10,000 s continuous operation, suggesting lower stability/durability than the Co_3O_4/N-rmGO hybrid. Activity instability of metal-N/C catalysts in acidic electrolyte is also well known and has been a limiting factor to the practical use of this material[6,7]. Pt catalyst is known to gradually degrade over time because of surface oxides and particle dissolution and aggregation, especially in the alkaline electrolytes used for alkaline fuel cells[4,34]). Long-term stabilities of other ORR catalysts, such as Ag in alkaline solutions, are improved over Pt, but still suffer from deactivation and are below the targets for applications[29]. As the lack of catalyst durability has been one of the major challenges for alkaline fuel cells, the excellent stability of our Co_3O_4/N-rmGO hybrid makes it promising for ORR and other important catalytic reactions in alkaline solutions[35].

We performed X-ray absorption near edge structure (XANES) measurements to glean the interactions between Co_3O_4 and GO in our hybrids (Fig. 1f). Compared to N-rmGO, Co_3O_4/N-rmGO hybrid showed a clear increase of carbon K-edge peak intensity at ~288 eV, corresponding to carbon atoms in graphene attached to oxygen or other species[36,37]. This suggested the possible formation of interfacial Co–O–C and Co–N–C bonds in the Co_3O_4/N-rmGO hybrid. In the oxygen K-edge XANES, an obvious decrease in unoccupied O 2p–Co 3d hybridized state (~532 eV; ref. 38) was observed (Fig. 1f inset), accompanied by an increase in the Co L-edge XANES (mapping of the unoccupied Co 3d projected state, see Supplementary Fig. S10) peak[38] in the hybrids compared to pure Co_3O_4 nanocrystal, suggesting a higher electron density at the O site and a lower electron density at the Co site, and consequently a higher ionic Co–O bonding in the hybrid[39]. Bond formation between Co_3O_4 and N-rmGO (as suggested by C K-edge XANES) and changes in the chemical bonding environment for C, O and Co atoms in the hybrid material are probably responsible for the synergistic ORR catalytic activity.

N-doping of GO could afford stronger coupling between Co and graphene in Co_3O_4/N-rmGO than in Co_3O_4/rmGO. N-groups on reduced GO serve as favourable nucleation and anchor sites for Co_3O_4 nanocrystals owing to coordination with Co cations[24]. This is consistent with a smaller Co_3O_4 nanocrystal size (higher degree of nucleation) on N-rmGO than on rmGO. Electronic effects of N-doping of graphene could also play a role in ORR. Note that Metal-N species is believed to be ORR-active sites in Fe- or Co-N/C catalysts[7] prepared at much higher temperatures (600–1,000 °C) with much lower metal loadings (<1–2 at% of metal; ref. 7). Our hybrid catalysts exhibit higher stability and differ in low temperature solution-phase synthesis and the Co in our hybrid is in the form of oxides (see XPS in Supplementary Fig. S2d) with a high Co loading of ~20 at%. Lowering the Co loading to 3–10 at% in our Co_3O_4/N-rmGO catalyst led to systematic reduction in ORR activity (Supplementary Fig. S11), suggesting that the active reaction sites in our hybrid materials could be Co oxide species at the interface with graphene.

The mechanism of ORR with our hybrid catalyst remains unclear. The Tafel slope of kinetic current down to ~37 mV/decade for Co_3O_4/N-rmGO in 1 M KOH is among the lowest for spinel oxide ORR catalysts and close to $2.303(2RT/3F)$ V/decade (R, universal gas constant; F, Faraday constant), suggesting protonation of O_2^- on the active sites of catalyst as the rate limiting step[40]. A dual-site mechanism has been proposed for cobalt-polypyrrole/C ORR catalyst, in which oxygen is reduced to peroxide at Co–N–C sites and further reduced to OH^- at Co_xO_y/Co sites[41]. A similar mechanism may be at work in our hybrid system. However, we note that Co_3O_4/rmGO without any N species has very similar ORR onset potential to Co_3O_4/N-rmGO, suggesting that the active sites may not directly involve N species in the hybrids but are enhanced by N doping of mGO. It is also found that physical mixtures of Co_3O_4 with rmGO or N-rmGO afforded much lower ORR activities than the corresponding hybrid material (Supplementary Fig. S12), suggesting synergistic coupling between Co_3O_4 and graphene is indispensable to the high ORR activity of the hybrid.

We also used the same method to prepare Co_3O_4 hybrids with other forms of carbon and compared their ORR performances

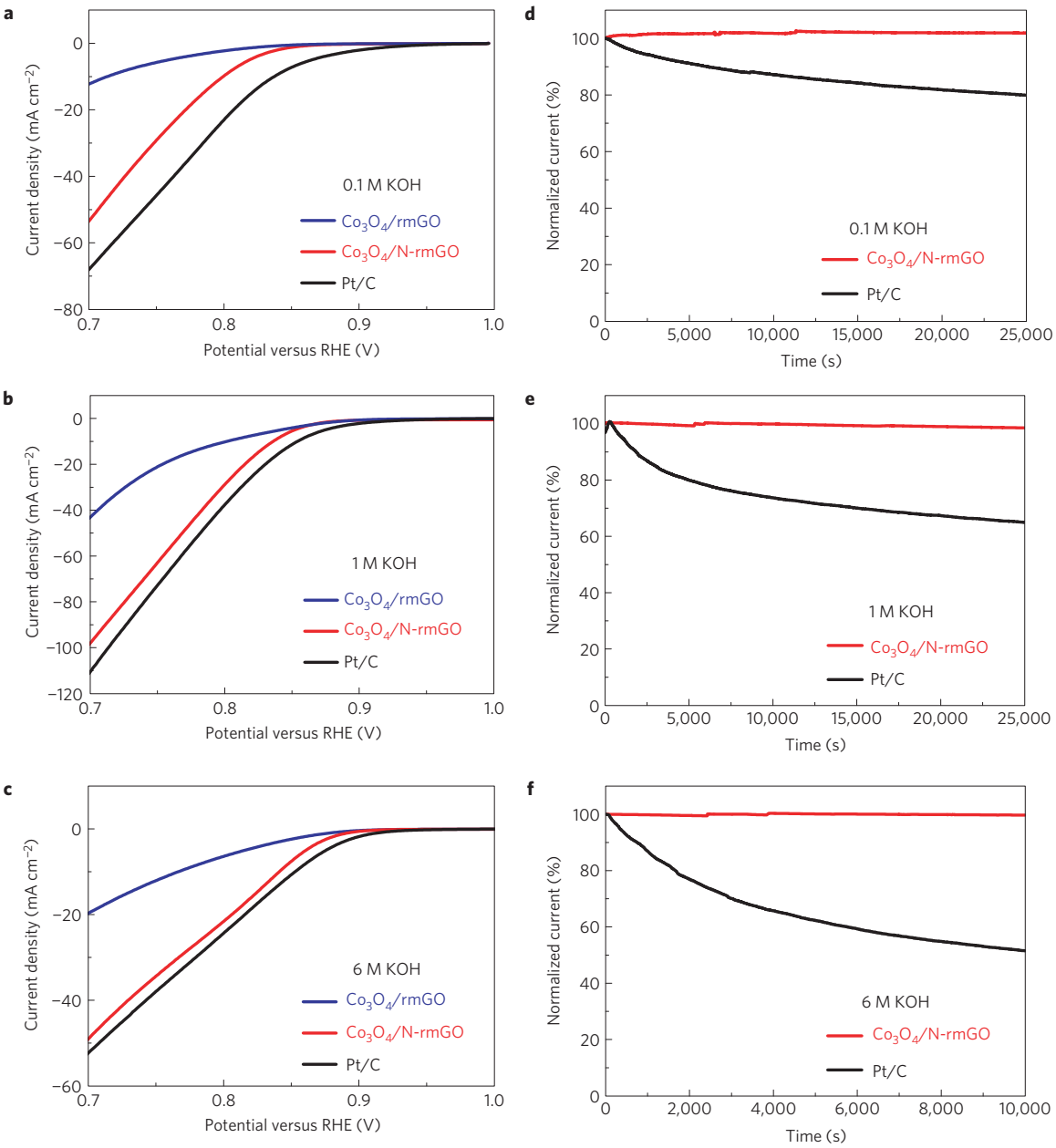

Figure 4 | ORR performance and stability of catalysts. a–c, Oxygen reduction polarization curves of Co_3O_4/rmGO, Co_3O_4/N-rmGO and a high quality commercial Pt/C catalyst (catalyst loading ~0.24 mg cm^{-2} for all samples) dispersed on CFP in O_2-saturated (**a**) 0.1 M KOH, (**b**) 1 M KOH and (**c**) 6 M KOH electrolytes respectively. **d–f**, Chronoamperometric responses (percentage of current retained versus operation time) of Co_3O_4/N-rmGO hybrid and Pt/C on carbon fibre paper electrodes kept at 0.70 V versus RHE in O_2-saturated (**d**) 0.1 M KOH, (**e**) 1 M KOH and (**f**) 6 M KOH electrolytes respectively. The Co_3O_4/N-rmGO hybrid showed comparable ORR catalytic activity to Pt/C and superior stability in alkaline solutions.

(Supplementary Fig. S13). The result indicated that high conductivity, high surface area, and suitable functional groups on carbon materials are important for the high activity of hybrid materials.

Lastly, we extended the potential of our hybrid electrode to 1.70 V versus RHE to the water oxidation regime and evaluated electrocatalytic oxygen evolution reaction (OER). In 0.1 M KOH, the same sample used for ORR containing Co_3O_4/N-rmGO loaded on CFP (at 0.24 mg cm^{-2}) afforded higher OER currents than either free Co_3O_4 nanocrystals or Pt/C (Fig. 5a). Furthermore, we loaded our Co_3O_4/N-rmGO catalyst onto Ni foam at ~1 mg cm^{-2} and evaluated OER performance in 1 M KOH at room temperature (Fig. 5b). Our catalyst afforded a current density of 10 mA cm^{-2} at a small overpotential of ~0.31 V (Fig. 5b) and a small Tafel slope down to 67 mV/decade (Fig. 4c), comparable to the performance of the best reported Co_3O_4 nanoparticle OER catalyst at the same loading[42]. N-doping of graphene did not affect OER activity, as Co_3O_4/rmGO hybrid showed only slightly lower OER activity than Co_3O_4/N-rmGO (Fig. 5b). Stability tests on glassy carbon electrodes showed that both Co_3O_4/N-rmGO and Co_3O_4/rmGO hybrids are inherently stable during OER cycling (Supplementary Fig. S14). These results make our hybrid material a powerful bi-functional catalyst for both oxygen reduction and water oxidation. Previously, manganese oxide was shown to be a bi-functional catalyst for ORR and OER (ref. 15). Our Co_3O_4/N-rmGO catalyst outperforms manganese oxide with smaller over-potentials for both ORR and OER, presenting the highest performance non-precious metal-based bi-functional catalyst.

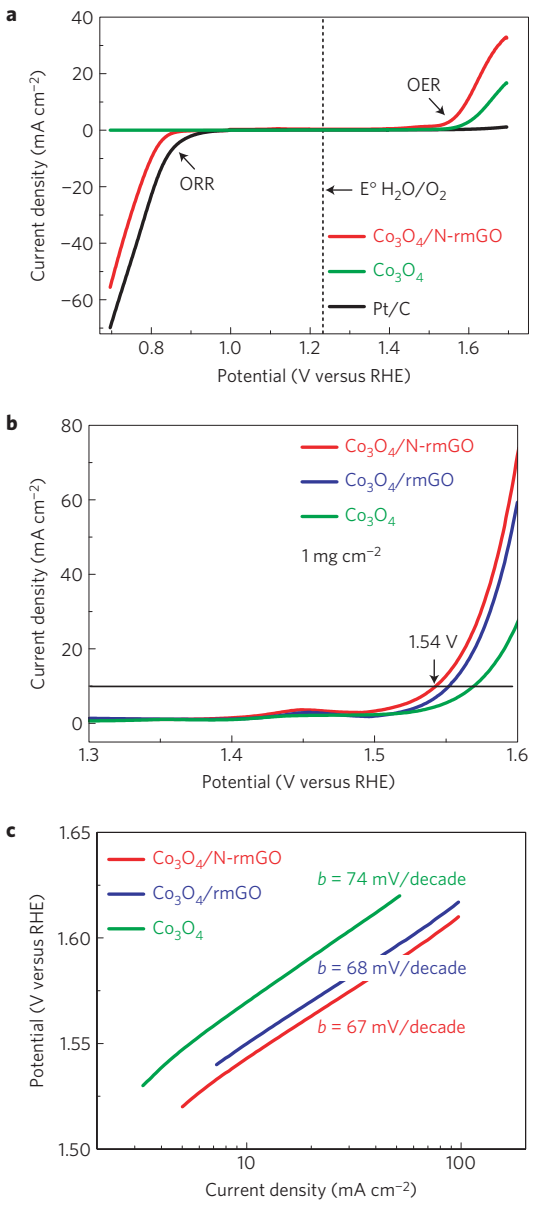

Figure 5 | Co_3O_4/graphene hybrid bi-functional catalyst for ORR and water oxidation (OER). a, Oxygen electrode activities within the ORR and OER potential window of Co_3O_4/N-rmGO hybrid, Co_3O_4 nanocrystal and Pt/C catalysts (catalyst loading ~0.24 mg cm^{-2} for all samples) dispersed on carbon fibre paper in O_2-saturated 0.1 M KOH. Co_3O_4/N-rmGO hybrid showed excellent catalytic activities for both ORR and OER. Free Co_3O_4 showed little ORR activity whereas Pt/C showed little OER activity. **b**, Oxygen evolution currents of Co_3O_4/N-rmGO hybrid, Co_3O_4/rmGO hybrid and Co_3O_4 nanocrystal loaded onto Ni foam (to reach a high catalyst loading of ~1 mg cm^{-2}) measured in 1 M KOH. **c**, Tafel plots of OER currents in **b**.

In summary, although Co_3O_4 or graphene oxide alone have little catalytic activity for ORR, their hybrid materials exhibit unexpected, surprisingly high ORR activities in alkaline solutions, comparable to fresh commercial Pt/C catalyst but far exceeding Pt/C in stability and durability. This presents a highly promising catalyst for alkaline fuel cells for which there has been a recent resurgence in interest as a solution to electrolyte carbonation[35]. We also demonstrated a Co_3O_4/graphene hybrid as one of the rare and highest performance bi-functional catalysts for ORR and water oxidation/OER. Thus, synergistic coupling of nanomaterials opens up a brand new approach to advanced catalysts for energy conversion.

Methods

Materials synthesis. GO was made by a modified Hummers method, in which a six times lower concentration of $KMnO_4$ was used than that for Hummers' GO. In the first step of Co_3O_4/rmGO hybrid synthesis, $Co(OAc)_2$ aqueous solution was added into GO/ethanol dispersion at room temperature. The reaction was stirred for 10 h at 80 °C. In the second step, the reaction mixture from the first step was transferred to an autoclave for hydrothermal reaction at 150 °C for 3 h. To synthesize Co_3O_4/N-rmGO, NH_4OH was added after $Co(OAc)_2$ addition in the first step. See Supplementary Information for detailed experimental procedures.

Electrochemical measurements. A saturated calomel electrode was used as the reference electrode in all measurements and was calibrated with respect to a reversible hydrogen electrode (see Supplementary Information for details). Cyclic voltammetry was conducted in a three-electrode electrochemical cell using a graphite rod as the counter electrode. 12 μg of sample was loaded on the glassy carbon working electrode (3 mm in diameter). In the rotating disk electrode and rotating ring-disk electrode measurements, the working electrode was prepared by loading 20 μg of sample on a glassy carbon electrode of 5 mm in diameter (0.1 mg cm^{-2}). For the measurement on carbon fibre paper, the working electrode was prepared by loading 0.24 mg of sample on 1 cm^2 carbon fibre paper from its ethanol dispersion with Nafion (10% to sample). All the data from carbon fibre paper were iR-compensated. The scan rate was 5 mV s^{-1} for all electrochemical measurements.

Characterizations. Scanning electron microscopy was carried out on an FEI XL30 Sirion scanning electron microscope. Transmission electron microscopy was carried out on an FEI Tecnai G2 F20 transmission electron microscope. X-ray diffraction (XRD) was carried out on a PANalytical X'Pert instrument. XPS was carried out on an SSI S-Probe XPS Spectrometer. The XANES at the C K-edge, O K-edge and Co L-edge were obtained on the spherical grating monochromator (SGM) beamline ($E/\Delta E \sim 5{,}000$) at the Canadian Light Source (CLS), a 2.9 GeV third generation synchrotron source.

Received 21 December 2010; accepted 30 June 2011; published online 7 August 2011

References

1. Lewis, N. S. & Nocera, D. G. Powering the planet: Chemical challenges in solar energy utilization. *Proc. Natl Acad. Sci.* **103,** 15729–15735 (2006).
2. Bard, A. J. & Fox, M. A. Artificial photosynthesis—solar splitting of water to hydrogen and oxygen. *Acc. Chem. Res.* **28,** 141–145 (1995).
3. Winter, M. & Brodd, R. J. What are batteries, fuel cells, and supercapacitors? *Chem. Rev.* **104,** 4245–4269 (2004).
4. Gewirth, A. A. & Thorum, M. S. Electroreduction of dioxygen for fuel-cell applications: Materials and challenges. *Inorg. Chem.* **49,** 3557–3566 (2010).
5. Bashyam, R. & Zelenay, P. A class of non-precious metal composite catalysts for fuel cells. *Nature* **443,** 63–66 (2006).
6. Lefevre, M., Proietti, E., Jaouen, F. & Dodelet, J-P. Iron-based catalysts with improved oxygen reduction activity in polymer electrolyte fuel cells. *Science* **324,** 71–74 (2009).
7. Bezerra, C. W. B. *et al.* A review of Fe-N/C and Co-N/C catalysts for the oxygen reduction reaction. *Electrochim. Acta* **53,** 4937–4951 (2008).
8. Gong, K., Du, F., Xia, Z., Durstock, M. & Dai, L. Nitrogen-doped carbon nanotube arrays with high electrocatalytic activity for oxygen reduction. *Science* **323,** 760–764 (2009).
9. Liu, R., Wu, D., Feng, X. & Muellen, K. Nitrogen-doped ordered mesoporous graphitic arrays with high electrocatalytic activity for oxygen reduction. *Angew. Chem. Int. Edn.* **49,** 2565–2569 (2010).
10. Qu, L., Liu, Y., Baek, J-B. & Dai, L. Nitrogen-doped graphene as eficient metal-free electrocatalyst for oxygen reduction in fuel cells. *ACS Nano* **4,** 1321–1326 (2010).
11. Nocera, D. G. Chemistry of personalized solar energy. *Inorg. Chem.* **48,** 10001–10017 (2009).
12. Kanan, M. W. & Nocera, D. G. *In situ* formation of an oxygen-evolving catalyst in neutral water containing phosphate and Co^{2+}. *Science* **321,** 1072–1075 (2008).
13. Trasatti, S. *Electrodes of Conductive Metal Oxides* (Elsevier, 1980).
14. Chen, G., Bare, S. R. & Mallouk, T. E. Development of supported bifunctional electrocatalysts for unitized regenerative fuel cells. *J. Electrochem. Soc.* **149,** A1092–A1099 (2002).
15. Gorlin, Y. & Jaramillo, T. F. A bifunctional nonprecious metal catalyst for oxygen reduction and water oxidation. *J. Am. Chem. Soc.* **132,** 13612–13614 (2010).
16. Wang, H., Robinson, J. T., Diankov, G. & Dai, H. Nanocrystal growth on graphene with various degrees of oxidation. *J. Am. Chem. Soc.* **132,** 3270–3271 (2010).

17. Wang, H. L., Casalongue, H. S., Liang, Y. Y. & Dai, H. J. Ni(OH)$_2$ nanoplates grown on graphene as advanced electrochemical pseudocapacitor materials. *J. Am. Chem. Soc.* **132,** 7472–7477 (2010).
18. Liang, Y. Y., Wang, H. L., Casalongue, H. S., Chen, Z. & Dai, H. J. TiO$_2$ nanocrystals grown on graphene as advanced photocatalytic hybrid materials. *Nano Res.* **3,** 701–705 (2010).
19. Li, Y. *et al.* MoS$_2$ nanoparticles grown on graphene: An advanced catalyst for the hydrogen evolution reaction. *J. Am. Chem. Soc.* **133,** 7296–7299 (2011).
20. Wang, H. *et al.* Advanced asymmetrical supercapacitors based on graphene hybrid materials *Nano Res.*http://dx.doi.org/10.1007/s12274-011-0128-7 (2011).
21. Wang, H. *et al.* Mn$_3$O$_4$-graphene hybrid as a high-capacity anode material for lithium ion batteries. *J. Am. Chem. Soc.* **132,** 13978–13980 (2010).
22. Nethravathi, C. & Rajamathi, M. Chemically modified graphene sheets produced by the solvothermal reduction of colloidal dispersions of graphite oxide. *Carbon* **46,** 1994–1998 (2008).
23. Dong, Y., He, K., Yin, L. & Zhang, A. A facile route to controlled synthesis of Co$_3$O$_4$ nanoparticles and their environmental catalytic properties. *Nanotechnology* **18,** 435602 (2007).
24. Cotton, F. A., Wikinson, G. & Murillo, C. A. *Advanced Inorganic Chemistry* (Wiley, 1999).
25. Long, D. *et al.* Preparation of nitrogen-doped graphene sheets by a combined chemical and hydrothermal reduction of graphene oxide. *Langmuir* **26,** 16096–16102 (2010).
26. Mayrhofer, K. J. J. *et al.* Measurement of oxygen reduction activities via the rotating disc electrode method: From Pt model surfaces to carbon-supported high surface area catalysts. *Electrochim. Acta* **53,** 3181–3188 (2008).
27. Bard, A. J. & Faulkner, L. R. *Electrochemical Methods: Fundamentals and Aplications* (Wiley, 2001).
28. Paulus, U. A., Schmidt, T. J., Gasteiger, H. A. & Behm, R. J. Oxygen reduction on a high-surface area Pt/Vulcan carbon catalyst: A thin-film rotating ring-disk electrode study. *J. Electroanal. Chem.* **495,** 134–145 (2001).
29. Bidault, F., Brett, D. J. L., Middleton, P. H. & Brandon, N. P. Review of gas diffusion cathodes for alkaline fuel cells. *J. Power Sources* **187,** 39–48 (2009).
30. Mehta, V. & Cooper, J. S. Review and analysis of PEM fuel cell design and manufacturing. *J. Power Sources* **114,** 32–53 (2003).
31. Escribano, S., Blachot, J-F., Etheve, J., Morin, A. & Mosdale, R. Characterization of PEMFCs gas diffusion layers properties. *J. Power Sources* **156,** 8–13 (2006).
32. Piana, M., Catanorchi, S. & Gasteiger, H. A. Kinetics of non-platinum group metal catalysts for the oxygen reduction reaction in alkaline medium. *Electrochem. Soc. Trans.* **16,** 2045–2055 (2008).
33. Meng, H., Jaouen, F., Proietti, E., Lefevre, M. & Dodelet, J. P. pH-effect on oxygen reduction activity of Fe-based electro-catalysts. *Electrochem. Commun.* **11,** 1986–1989 (2009).
34. Jin, W., Du, H., Zheng, S. L., Xu, H. B. & Zhang, Y. Comparison of the oxygen reduction reaction between NaOH and KOH solutions on a Pt electrode: The electrolyte-dependent effect. *J. Phys. Chem. B* **114,** 6542–6548 (2010).
35. Spendelow, J. S. & Wieckowski, A. Electrocatalysis of oxygen reduction and small alcohol oxidation in alkaline media. *Phys. Chem. Chem. Phys.* **9,** 2654–2675 (2007).
36. Zhang, L-S., Liang, X-Q., Song, W-G. & Wu, Z-Y. Identification of the nitrogen species on N-doped graphene layers and Pt/NG composite catalyst for direct methanol fuel cell. *Phys. Chem. Chem. Phys.* **12,** 12055–12059 (2010).
37. Zhou, J. G. *et al.* Immobilization of RuO$_2$ on carbon nanotube: An x-ray absorption near-edge structure study. *J. Phys. Chem. C* **113,** 10747–10750 (2009).
38. Rojas, T. C. *et al.* Preparation, characterization and thermal evolution of oxygen passivated nanocrystalline cobalt. *J. Mater. Chem.* **9,** 1011–1017 (1999).
39. Zhou, J. G. *et al.* Electronic structure of TiO$_2$ nanotube arrays from X-ray absorption near edge structure studies. *J. Mater. Chem.* **19,** 6804–6809 (2009).
40. De Koninck, M. & Marsan, B. Mn$_x$Cu$_{1-x}$Co$_2$O$_4$ used as bifunctional electrocatalyst in alkaline medium. *Electrochim. Acta* **53,** 7012–7021 (2008).
41. Olson, T. S. *et al.* Anion-exchange membrane fuel cells: Dual-site mechanism of oxygen reduction reaction in alkaline media on cobalt-polypyrrole electrocatalysts. *J. Phys. Chem. C* **114,** 5049–5059 (2010).
42. Esswein, A. J., McMurdo, M. J., Ross, P. N., Bell, A. T. & Tilley, T. D. Size-dependent activity of Co$_3$O$_4$ nanoparticle anodes for alkaline water electrolysis. *J. Phys. Chem. C* **113,** 15068–15072 (2009).

Acknowledgements

We thank T.F. Jaramillo for insightful discussions. This work was supported in part by ONR. CLS is supported by the NSERC, NRC, CIHR of Canada, and the University of Saskatchewan.

Author contributions

Y. Liang, Y. Li, H.W. and H.D. conceived the project and designed the experiments. Y. Liang, Y. Li and H.W. performed the experiments. J.Z., J.W. and T.R. performed the XANES measurement and analysis. Y. Liang, Y. Li, H.L. and H.D. analysed the data. Y. Liang, Y. Li and H.D. co-wrote the paper. All authors discussed the results and commented on the manuscript.

Additional information

The authors declare no competing financial interests. Supplementary information accompanies this paper on www.nature.com/naturematerials. Reprints and permissions information is available online at http://www.nature.com/reprints. Correspondence and requests for materials should be addressed to H.D.